Oscillatory Neural Networks for Robotic Yoyo Control

This work has been conditionally accepted by the IEEE Transactions on Neural Networks *for possible publication. Copyright may be transfered without notice, after which this version may no longer be accessible.*

Hui-Liang Jin and M. Zacksenhouse

Hui-Liang Jin and M. Zacksenhouse are both with the Sensory-Motor Integration Laboratory, Faculty of Mechanical Engineering, Technion-Israel Institute of Technology, Haifa 32000, Israel (e-mail: hlj@tx.technion.ac.il; mermz@tx.technion.ac.il)

Abstract

Different networks of coupled oscillators were developed for open-loop control of periodic motion. However, some tasks, like yoyo playing, are open-loop unstable and require proper phase locking to stabilize. Given the phase-locking property of coupled oscillators, we investigate their application to closed-loop control open-loop unstable systems, concentrating on the challenging task of yoyo control. In particular, we focus on pulse-coupling, where the yoyo sends a feedback upon reaching the bottom of the string and the onset of the oscillatory cycle is used to trigger the movement. Four networks involving either a stand-alone or a circuit level oscillator with either excitatory or inhibitory couplings are considered. Working curve analysis indicates that three of the networks cannot stabilize the yoyo. The fourth network, which is based on a circuit-level oscillator, is analyzed using the return map and the region of stability is determined and verified by simulations. The resulting pulse-coupled oscillatory control provides a model-free control strategy that operates with an easy-to-measure low-rate feedback.

Keywords: Yoyo control, Rhythmic movements, Phase-locked loops, Oscillators, CPGs.

I. Introduction

Experimental investigations of the neural systems underlying the rhythmic activities of biological systems, such as walking, swimming and chewing, led to the notion of *central pattern generator*, or briefly CPG [1], [2], [3], [4], [5]. CPGs consist of groups of neurons (usually in the spinal cord or ganglia) that collectively release sequences of cyclic excitations [6]. It is hypothesized that the observed rhythmic motion is an effect of CPG activity.

For the past two decades, a number of *oscillatory neural networks* (ONN) have been developed to model biological CPGs. Examples include the model of the gastric mill CPG that controls the chewing movements of the lobster [7], and the model of the lamprey CPG that controls the swimming movements [8]. While the oscillatory units in these models represent specific neurons, in other models they represent groups of neurons or subsystems that collectively generate the motion. Examples include the models for finger tapping [9], [10], and those for bipedal or

quadrupedal locomotion [6], [11].

The characteristic behavior of these oscillatory networks emerges from the mutual coupling between closely tuned intrinsic oscillators. The coupling evokes phase locking, i.e., all the oscillators eventually oscillate at a single frequency and maintain a constant pattern of relative phases [8], [7]. Furthermore, with a different set of parameters, the same network may oscillate at a different frequency with a different pattern of relative phases. Each pattern of relative phases gives rise to a particular pattern of steady state movement, so one oscillatory neural network may produce multiple patterns of movement [12], [6], [9], [10].

The output of the oscillatory neural network may be either continuous or discrete, corresponding to either the voltage or the spikes elicited by specific oscillators. When applied to control, the continuous output is used directly as a reference trajectory of the controlled variable [13], [14], [11], while the discrete output is used to trigger the pre-designed motion of the actuators [12], [6].

In most of these models, it is explicitly or implicitly assumed that the net driving signal to the CPG consists only of descending influences from higher level central nervous system [6, p383] and [14, p906]. However, several recent experimental studies have shown that CPGs may also receive afferent inputs from peripheral sensory organs [15], [16], [14]. Furthermore, neural oscillators have been hypothesized to participate in temporal pattern detection as part of neural phase-locked loop [17]. Thus neural oscillators may provide the basis for both temporal pattern generation and temporal pattern detection [18].

The characteristics and hypothesized role of ONNs for generating rhythmic movements in biological systems have motivated the development of ONNs for robot control. The coupling between the intrinsic oscillators was investigated to develop networks that can generate different stable gaits for biped [13], quadruped [19], and hexapod [12] robots. Applications to rhythmic arm movements focused on the coupling between the ONN and the dynamics of the arm, which

was modeled as an open-loop stable pendulum [20], [21], and on the coupling between to ONNs through the dynamics of the held object [22].

Encouraged by the development of various models of oscillators and their applications in open-loop control of rhythmic motion, we investigate their application to closed-loop control of open-loop unstable systems. Yoyo playing is considered as a representative example of open-loop unstable control problems that involve intermittent dynamical environments. Stable control of yoyo playing relies on a proper phase relationship between the action of the controller and the motion of the yoyo. Given the phase-locked property of coupled oscillators, we investigate the possibility of controlling the yoyo by properly coupling it to an oscillator. Successful control of robotic yoyo playing with a neural oscillator provides a model-free alternative to the model-based control of such tasks.

In Section II, we present different configurations for coupling the yoyo and the neural oscillator and the specific configuration that will be explored in this paper. The system is functionally divided into several blocks and mathematically modeled accordingly. In Section III, we review the open-loop response of four oscillatory networks involving either a stand-alone or circuit level oscillator with either excitatory or inhibitory coupling. The resulting working curves are evaluated against the working curve of the yoyo, and it is concluded that three of the four networks cannot stabilize the yoyo. In Section IV, we derive the closed-loop return map of the fourth network and analyze the fixed point and its local stability. Numerical simulations for verifying the analytic results are presented in Section V. We conclude in Section VI, and discuss basic methodologies of open-loop versus closed-loop control and oscillator-based versus model-based control.

II. Control configuration and Modeling

When operating a yoyo, a skilled player can compensate the pitching, yawing and swinging while keeping the yoyo rolling up-and-down along the string. We assume that human skills in yoyo playing include two levels. The low level skill involves moving the hand up and down at the right phase of the yoyo motion, while the high level skill involves compensating the pitching, yawing and swinging. In this project, we shall restrict ourselves to the low level control, and in particular to the *stability of the vertical movement*.

A. Configuration

Two coupled oscillators form the basic building block of CPGs [7], [22], [10]. Different types of oscillators may be used without significantly affecting the overall behavior [6]. The coupling between the two oscillators may be classified as (1) *linear coupling*, where the input to one oscillator is a linear function of the output from the other oscillator [6], [11], (2) *synaptic coupling*, where the input to one oscillator is a nonlinear function of the output from the other oscillator [13], [7], or (3) *impulsive coupling*, where the input to one oscillator is only an impulse, called a spike or an event, generated from the output of the other oscillator [17], [23], [18]. Moreover, a coupling is said to be *inhibitory* (or *excitatory*) if it tends to prolong (or shorten, respectively) the period of the oscillator.

Motivated by the oscillatory, albeit damped, nature of the yoyo, we shall investigate the possibility of coupling the yoyo to a neural oscillator in a closed-loop as shown in Fig. 1a. Several configurations of the oscillator-based control are possible, depending on the type of coupling and the nature of the oscillator. Specifically, we consider either single neural oscillators or phase-locked loops (PLLs), which operate as circuit level oscillators. PLLs are well known electric circuits for decoding temporal information [24], and may be implemented by different neural circuits [17], [25]. Their structure endows them with special properties [18], which are exploited

in this paper in the context of yoyo control.

(Fig. 1 here)

We shall consider only the impulsive coupling, which is both natural to the task and advantageous in terms of the required feedback rate. The yoyo generates an impulse of force upon reaching the bottom of the string. Similarly, the oscillator generates an impulse (spike) at a specific phase of its cycle. The impulse from the oscillator triggers the upward acceleration of the robot, while the impulse from the yoyo signals the robot to return to its origin (Fig. 1b).

B. Oscillatory units

Models of *single neuron* oscillators are captured by a first or second order nonlinear differential equation with at least one stable periodic solution. Different models have been suggested, including the Van der Pol relaxation oscillator [6], [9], [7], [11], the Stein oscillator [6], and the leaky integrate-and-fire (LIF) oscillator [13], [12], [6], [26], [18]. As a simple but representative single-neuron model, we consider the LIF oscillator described in [18] with either inhibitory (iLIF) or excitatory (eLIF) coupling.

(Fig. 2 here)

A PLL includes an intrinsic oscillator, which is connected to the input indirectly via a phase-detector (PD) as shown in Fig. 2b. The PD compares the output of the intrinsic oscillator, whose impulses are referred to as the internal events, with the external input, whose impulses are referred to as the external events, and generates a signal representing their phase relationship. The output from the PD is fed into the intrinsic oscillator and may have either inhibitory (iPLL) or excitatory (ePLL) effect. As a result, the intrinsic oscillator can track the period of the input and respond to its variations. Special properties of PLLs, which distinguish them from single-neuron oscillators, emerge when the PD is sensitive to the correlation, instead of difference, between the two inputs [18]. A particular correlation-based PD, which responds continuously as

long as the external and internal events occur within the preceding time window T_w, is depicted in Fig. 2c. Specifically, each impulse triggers a unit square wave of fixed duration T_w, and the output of the PD is the product of the two square waves. In the sequel, we shall consider PLLs with LIF intrinsic oscillators and correlation based PDs.

C. Switching control algorithm

The oscillator provides only a timing signal, which triggers the upward movement of the robot. Once initiated, the stereotypical movement continues with a constant acceleration until the yoyo hits the bottom. To simplify the analysis, we neglect the dynamics of the robot by assuming that the robot can track exactly the following trajectory

$$\ddot{h} = \begin{cases} \kappa g & \text{for } s(t) = 1 \\ -c_1\dot{h} - c_2 h & \text{for } s(t) = 0 \end{cases} \tag{1}$$

where $\kappa > 0$, $c_1 \geq 0$ and $c_2 > 0$ are pre-designed constant parameters, and g is the gravitational constant. The trjectory $h(t)$ specifies the vertical position of robot "holding" the string of the yoyo. The parameter κ determines the magnitude of upward acceleration and greatly affects the amplitude of the yoyo as will be discussed in Section III. The other two parameters c_1 and c_2 are the differential and proportional gains, which should be designed to smoothly return the robot to its origin with no severe overshoot and before the yoyo reaches the next top position. The switching signal $s(t)$ is set by the oscillator and reset by the output from the yoyo as described below.

D. Switching signal generator

The switching signal generator receives the output of the oscillator and the "hit bottom" impulse from the yoyo. We denote by t_j the time at which the yoyo hits the bottom during j-th cycle, and T_j the time at which the oscillatory event occurs during that cycle.

D.1 Switching signal generation from LIF oscillators

The output of the LIF is the train of impulses generated by the oscillator at $\{T_j\}$. Based on this information, the switching signal is set at the time of the impulse and is reset immediately after the yoyo reaches the bottom. Thus

$$s(t) = \begin{cases} 1 & \text{for } T_j \le t < t_j,\ j = 1, 2, \cdots \\ 0 & \text{otherwise} \end{cases} \tag{2}$$

A fixed delay may be added without affecting the subsequent analysis.

D.2 Switching signal generation from PLLs

The PLL enforces specific phase relationships between the internal and external events [18]. Particularly, the internal events in an ePLL lead the external events, whereas the internal events in an iPLL lag the external events. Furthermore, the response of the PD starts after the occurrence of the later input (the external or internal event in ePLL or iPLL, respectively) and lasts until a time window T_w has elapsed from the occurrence of the earlier input.

Thus the impulses generated by an ePLL occur within the time window T_w before the yoyo hits the bottom, and may be used to generate the switching signal according to (2). In contrast, the impulses generated by an iPLL occur within the time window T_w after the yoyo hit the bottom, $t_j < T_j < t_j + T_w$, and thus too soon to set the switching signal on. In this case, it is necessary to delay the initiation of the switching signal beyond the extent of the response of the PD. Once initiated, the swithing signal lasts until the next time the yoyo hit the bottom at t_{j+1} (see also Fig. 4). So the delay may depend on the duration δ_j of the PD response, and for simplicity, is designed to be propotional to δ_j.

$$s(t) = \begin{cases} 1 & \text{for } T_j + (c+1)\delta_j \le t < t_{j+1},\ j = 1, 2, \cdots \\ 0 & \text{otherwise} \end{cases} \tag{3}$$

where $c > 0$ is a constant coefficient (we shall fix $c = 2$ to simplify the analysis in Section IV-C).

E. Yoyo model

The simple one-degree of freedom (DOF) model developed in [27] is used for analyzing the control system. As described there, the one DOF model is derived from a more detailed two DOF model by capturing the dynamics at the bottom with an equivalent restitution effect e_{eq}. The one-DOF model adequately describes the total energy loss and is therefore sufficient for control analysis.

Let the mass and the inertia of the yoyo be m and I, the radii of the axle and the disk of the yoyo be r and R, respectively, the rotational angle be θ, the total length of the string be L, and the position of the yoyo center and the robot be y and h, respectively.

When the yoyo is rolling down the string, its dynamics is governed by [27]:

$$\begin{aligned} \ddot{\theta} &= -\gamma\,(g + \ddot{h}), \quad \text{for} \quad \theta(t) > 0 \\ y(t) &= h(t) - L + r\theta(t) \end{aligned} \tag{4a}$$

where $\gamma = mr/(I + mr^2)$. When the yoyo hits the bottom, its dynamics may be captured by a restitution effect:

$$\dot{\theta}(t_j^+) = -e_{eq}\dot{\theta}(t_j^-), \quad \text{for} \quad \theta(t_j) = 0 \tag{4b}$$

where $e_{eq} = 1 - 2mr^2/(I + mr^2)$ is the equivalent coefficient of restitution. Due to the impulsive nature of the restitution effect, the yoyo exerts an impulsive force on the string when it reaches the bottom. The impulsive force can be easily detected by a force detector. This is a once-per-cycle low rate feedback that greatly simplifies the sensing and processing as compared for example with visual feedback.

III. Open loop analysis

Before analyzing the stability of the closed loop system, the open-loop responses of the different oscillators and the yoyo are analyzed.

A. Oscillators

We briefly review the behavior of an oscillator in response to a train of external events with a constant period (see [18] for detailed analysis).

A.1 LIF oscillator

The membrane voltage of a LIF oscillator decays exponentially from its initial value v_0 to its equilibrium v_e. When the membrane voltage reaches a threshold level it generates a spike and resumes the initial voltage value. Let the decay time-constant be τ and assume the threshold is zero, $v_0 < 0$, and $v_e > 0$, the period of the resulting oscillation is $\tau_{osc} = \tau \ln(\rho)$ where $\rho = 1 - v_0/v_e > 1$.

An excitatory or inhibitory input event increases or decreases the membrane voltage respectively, and thus shortens or lengthens its period. The modified period depends not only on the strength of the input α ($\alpha > 0$ for eLIF, $\alpha < 0$ for iLIF) but also on its timing with respect to the cycle of the oscillator. When the input period is τ_{ip}, the dynamics of the time delay is given by

$$\tau_d(k+1) = \tau_d(k) - \tau_p(k) + \tau_{ip} \tag{5a}$$

$$\tau_p(k) = \tau_{osc} + \tau \ln\bigl(1 - \alpha e^{\tau_d(k)/\tau}\bigr) \tag{5b}$$

where $\tau_d \in [0, \tau_{osc}]$ is the time delay with respect to the most recent internal event and τ_p is the perturbed period.

In the $\tau_p\tau_d$-plane, the curve of function (5b) is referred to as the *working curve* of the oscillator. Typical working curves are illustrated in Fig. 3. The range of values of the modified period τ_p is

referred to as the *working range*. A train of input events at a constant period τ_{ip} would result in a 1:1 phase locking at the fixed point τ_d^* such that $\tau_p(\tau_d^*) = \tau_{ip}$ if τ_{ip} is within the working range. The fixed point is stable for iLIF and unstable for eLIF, so the corresponding working curve are plotted as solid and dashed lines, respectively.

(Fig. 3 here)

A.2 PLL oscillator

Consider a PLL with a LIF as the intrinsic oscillator, and the correlation based PD of Fig. 2c. Either ePLL or iPLL may achieve stable 1:1 locking provided that the period of the input train τ_{ip} is in the corresponding working range. In particular, τ_{ip} should be less than, or greater than τ_{osc} to entrain the ePLL or iPLL, respectively. Phase locking in ePLLs is characterized by lagging input and the dynamics of the time difference is given by

$$\tau_d(k+1) = \tau_d(k) - \tau_p(k) + \tau_{ip} \tag{6a}$$

$$\tau_p(k) = \tau_{osc} + \tau \ln\bigl(1 - \beta e^{T_w/\tau} + \beta e^{\tau_d(k)/\tau}\bigr) \tag{6b}$$

In contrast, phase locking in iPLLs is characterized by leading input and the dynamics of the time difference is given by

$$\tau_d(k+1) = \tau_d(k) + \tau_p(k) - \tau_{ip} \tag{7a}$$

$$\tau_p(k) = \tau_{osc} + \tau \ln\bigl(1 + \beta - \beta e^{(T_w - \tau_d(k))/\tau}\bigr) \tag{7b}$$

The parameter β defines the strength of the continuous input from the PD to the LIF. Note that $\tau_d \in [0, T_w]$ is positive and corresponds to the interval between the two events of a pair. Representative stable working curves for ePLL ($\beta > 0$) and iPLL ($\beta < 0$) are illustrated in Fig. 3.

B. Yoyo working curve

Under the control algorithm (1), the robot is either i) waiting, ii) accelerating upward or iii) returning smoothly to its origin. The three corresponding intervals are marked I, II and III respectively (as shown in Fig. 4). Denote the steady state value of these intervals by I^*, II^* and III^* and the steady state period by $T^* = I^* + \mathit{II}^* + \mathit{III}^*$. It can be shown that the ratio between the acceleration interval II^* and the period T^* is constant (see Appendix I-C). In particular,

$$\upsilon(\kappa, e_{eq}) \triangleq \frac{\mathit{II}^*}{T^*} = \frac{1 - e_{eq}}{2(1 + e_{eq})\kappa} > 0 \tag{8}$$

In the II^*T^*-plan, this relation defines a straight line passing through the origin with a positive slope υ. This line is referred to as the *working curve* of the yoyo.

(Fig. 4 here)

C. Static analysis

According to the proposed control algorithm, the interval II during which the robot accelerates upward is determined by the time difference τ_d. More specifically, according to the switching algorithm (2), the two intervals are identical $\mathit{II} = \tau_d$. In the case of (3), II is a linear function of τ_d, with slope c, and when the period of the yoyo is fixed, the bias is constant.

In steady state, the period of the yoyo T^* and the period of the oscillator τ_p^* should be equal. Thus, the overall closed-loop system must work at a fixed point where the working curve of the oscillator intersects the steady state curve of the yoyo, as marked by circles in Fig. 3.

In the case of the iLIF and ePLL, the slope of the working curve of the oscillator at the fixed point is higher than that of the yoyo, so the overall system behaves like a positive feedback system and the fixed point is unstable. Specifically, consider the case when due to some external disturbance the system operates at a period that is longer than the period at the fixed point. This may occur for example if the disturbance causes the robot to start accelerating after some fixed

delay. When the disturbance is removed, however, the interval during which the robot accelerates is excessive and thus the period of the yoyo would further increase, leading to instability. Indeed, rigorous formulation [28] proves that the iLIF and ePLL cannot stabilize the yoyo.

Since the eLIF is unstable under periodic input, this case is not investigated any further. Thus the only network that may stabilize the yoyo is the iPLL, which is further investigated next.

IV. Closed-loop analysis

The working curve of the iPLL (7b) can be simplified to a straight line by selecting $\beta = -1$, so

$$\tau_p = \tau_{osc} + T_w - \tau_d = \tau_{osc} + \delta \tag{9}$$

The rest of the analysis is based on this simplification.

A. Return map

Given the amplitude Θ_j at the beginning of the j-th cycle and the waiting interval I_j, the motion in the j-th cycle is completely determined (see detailed analysis in Appendix I-A). To facilitate the formulation, we introduce two auxiliary variables Δ_j and μ_j, defined such that

$$\Theta_j = \frac{\gamma g}{2}\Delta_j^2 \tag{10}$$

and

$$\begin{aligned} I_j &= f_1(\mu_j)\Delta_j \\ f_1(\mu) &= \sqrt{\mu}, \qquad (0 \le \mu \le 1) \end{aligned} \tag{11}$$

In fact, Δ_j is the free flight interval till the yoyo reaches the bottom when $h(t) \equiv 0$. The parameter μ_j is referred to as the waiting ratio, as it is the square of the ratio of the waiting interval I_j and the free flight interval Δ_j. These two relations may be regarded as a coordinate transformation. Thus, we choose Δ and μ along with δ as three independent state variables.

Proposition 1: Under control algorithm (1) and (3), the return map of a closely tuned system, where the period of the yoyo is close to the intrinsic period of the oscillator τ_{osc}, satisfies

$$\Delta_{j+1} = f_4(\mu_j; \kappa, e_{eq})\Delta_j \tag{12a}$$

$$f_1(\mu_{j+1})\Delta_{j+1} = T_w + c\delta_j - f_3(\mu_j; \kappa, e_{eq})\Delta_j \tag{12b}$$

$$\delta_{j+1} - f_2(\mu_{j+1}; \kappa)\Delta_{j+1} = T_w + c\delta_j - \tau_{osc} \tag{12c}$$

where

$$f_4(\mu; \kappa, e_{eq}) = \sqrt{f(\mu; \kappa, e_{eq})}$$

and f_1 is given in (11). The specific dependence of f, f_2, and f_3 on μ, κ, and e_{eq} are given in the Appendix, Eq. (27)-(28).

Proof: Applying the coordinate transformation (10) to equation (26) immediately yields (12a).

To prove (12b), we use the relation, shown in Fig. 4, that

$$\mathit{III}_j + I_{j+1} = (T_w - \delta_j) + (c+1)\delta_j \tag{13}$$

Using (29) and (11) in the above yields (12b).

To prove (12c), we use the relation shown in Fig. 4, that

$$\mathit{III}_j + I_{j+1} + \mathit{II}_{j+1} + (T_w - \delta_{j+1}) = (T_w - \delta_j) + \tau_p \tag{14}$$

Using (13) on the left-hand-side and (9) on the right-hand-side of this relation yields

$$T_w + c\delta_j + \mathit{II}_{j+1} - \delta_{j+1} = \tau_{osc} \tag{15}$$

Finally using (28) and reorganizing yields (12c). ■

For dimensionless analysis, we set $T_w = \xi_w \tau_{osc}$ (we fix $\xi_w = 0.4$) and introduce a coordinate transformation

$$x = \mu, \qquad y = \frac{\delta}{\tau_{osc}}, \qquad z = \frac{\Delta}{\tau_{osc}} \tag{16}$$

The return map (12) can be transformed into a new scaled system

$$z_{j+1} = f_4(x_j; \kappa, e_{eq}) z_j \tag{17a}$$

$$f_1(x_{j+1}) z_{j+1} = \xi_w + c y_j - f_3(x_j; \kappa, e_{eq}) z_j \tag{17b}$$

$$y_{j+1} - f_2(x_{j+1}; \kappa) z_{j+1} = \xi_w + c y_j - 1 \tag{17c}$$

The new system (17) is an autonomous discrete system in implicit form with two parameters κ and e_{eq}. Although an explicit form may be derived, we shall analyze the fixed point and its local stability directly on the implicit form. This is a key point to simplify the analysis in our system.

B. Fixed point

The next result presents the fixed point of this system.

Proposition 2: The discrete system (17) has a fixed point at (x^*, y^*, z^*) given by

$$x^* = \frac{\big((1+e_{eq})\kappa - (1-e_{eq})\big)^2}{\big((1+e_{eq})^2\kappa + (1-e_{eq})^2\big)\kappa} \tag{18a}$$

$$y^* = \frac{(1-\xi_w)(f_1^* + f_3^*) - \xi_w f_2^*}{(c-1)(f_1^* + f_3^*) + c f_3^*} \tag{18b}$$

$$z^* = \frac{1 + y^*}{f_1^* + f_3^* + f_2^*} \tag{18c}$$

where $f_1^* = f_1(x^*)$, $f_2^* = f_2(x^*; \kappa)$ and $f_3^* = f_3(x^*; \kappa, e_{eq})$.

Proof: Substitute the solution (18) for all the corresponding state variables in the return map (17) and check the equality. ■

C. Local stability of the fixed point

Local stability of the fixed point depends on the eigenvalues of the linearized system around the fixed point. Substituting the following coordinate transformation

$$x = x^* + \tilde{x}, \quad y = y^* + \tilde{y}, \quad z = z^* + \tilde{z} \tag{19}$$

in the return map (17), expanding on both sides to the first order, and neglecting higher order terms, yields

$$\begin{bmatrix} 1 & 0 & 0 \\ f_1^* & df_1^* & 0 \\ -f_2^* & -df_2^* & 1 \end{bmatrix} \boldsymbol{x}_{j+1} = \begin{bmatrix} 1 & df_4^* & 0 \\ -f_3^* & -df_3^* & c \\ 0 & 0 & c \end{bmatrix} \boldsymbol{x}_j \tag{20}$$

where $\boldsymbol{x} \triangleq [\tilde{z},\ z^*\tilde{x},\ \tilde{y}]^T$ and

$$df_i^* \triangleq \left.\frac{\partial f_i}{\partial \mu}\right|_{\mu=x^*}, \qquad i = 1, 2, 3, 4$$

Thus we get a linear system

$$\boldsymbol{x}_{j+1} = A\boldsymbol{x}_j \tag{21}$$

where

$$A = \begin{bmatrix} 1 & 0 & 0 \\ f_1^* & df_1^* & 0 \\ -f_2^* & -df_2^* & 1 \end{bmatrix}^{-1} \begin{bmatrix} 1 & df_4^* & 0 \\ -f_3^* & -df_3^* & c \\ 0 & 0 & c \end{bmatrix}$$

The characteristic equation of this matrix (setting $c = 2$ for simplification) is

$$a(\lambda) = |\lambda I - A| = \lambda^3 + a_2\lambda^2 + a_1\lambda + a_0 \tag{22}$$

where

$$a_2 = -(1 + e_{eq})^2\kappa - \frac{1}{2}(2e_{eq}^2 - 3e_{eq} + 3) \tag{23a}$$

$$a_1 = 2(1 + e_{eq})^2\kappa + \frac{1}{2}(3e_{eq}^2 - 5e_{eq} + 2) \tag{23b}$$

$$a_0 = e_{eq} - e_{eq}^2 \tag{23c}$$

To determine the range of parameters $(\kappa,\ e_{eq})$ for which the controlled yoyo is stable, we check Jury's criterion [29], which gives a necessary and sufficient condition for all the roots of a polynomial to be located in the unit circle. According to Jury's criterion, all the three roots of (22)

are located within the unit circle if and only if

$$a(1) = 1 + a_2 + a_1 + a_0 > 0 \tag{24a}$$

$$-a(-1) = 1 - a_2 + a_1 - a_0 > 0 \tag{24b}$$

$$|a_0| < 1 \tag{24c}$$

$$|a_1 - a_2 a_0| < |1 - a_0^2| \tag{24d}$$

Since $0 \leq e_{eq} < 1$ and $\kappa > 0$ for our system, it can be shown that conditions (24a), (24b) and (24c) are always satisfied and that condition (24d) is satisfied if and only if

$$\kappa < \kappa_s \triangleq \frac{e_{eq}}{2(1 + e_{eq})^2} \tag{25}$$

Since $x = \mu$ should be positive for physically meaningful solution, another condition, derived in Appendix I-B, states that $\kappa > \kappa_0$, where κ_0 is given by (32). Figure 5 shows the stability region $\kappa_0 < \kappa < \kappa_s$ in the κ-e_{eq} parameter space.

(Fig. 5 here)

Note that when

$$e_{eq} < \frac{\sqrt{17} - 1}{4} = 0.7808$$

$\kappa_s < \kappa_0$, and so the system cannot be stabilized regardless of κ.

V. Simulation results

We verify the fixed point and its stability for Yoyo-1 of [27] ($e_{eq} = 0.9183$, $\gamma = 0.0817$). The dependence of the fixed point (x^*, y^*, z^*) on κ is shown in Fig. 6b, where the solid and dashed parts indicate the stable and unstable regime, respectively. We have simulated the responses of the yoyo for different values of κ, within and outside the stability region.The simulations are conducted in MATLAB Simulink toolbox using the fourth order Runge-Kutta method with simulation step of 0.001 s. In all the simulations, $c_1 = 10$, $c_2 = 30$, $c = 2$.

The stability region of κ for this yoyo is between $\kappa_0 = 0.0425$ and $\kappa_s = 0.125$. For each value of κ within the stability region (Table I), the intrinsic period of the oscillator, τ_{osc}, is designed such that the amplitude of the yoyo is approximately 20 cm. The values of the amplitude of the

TABLE I

SELECTED κ AND τ_{osc} FOR SIMULATION

κ	0.0425	0.06	0.08	0.10	0.125
τ_{osc} (s)	1.84	1.67	1.56	1.50	1.45

yoyo, its period, and the waiting-time of the robot in the last ten cycles (for example Fig. 6a) are averaged to provide numerical results for x^*, y^* and z^*. The numerical results are plotted (as circles) in Fig. 6b and agree well with the analytical results. For the values of κ outside the stable region, the simulations indicate that the yoyo indeed becomes unstable and its amplitude either decays to zero or grows without bound.

(Fig. 6 here)

VI. DISCUSSION

We have studied the application of simple oscillatory neural networks for closed-loop control of yoyo. We considered four possible networks with either the LIF oscillator or the PLL oscillator and either excitatory or inhibitory coupling. The neural oscillator actuates a stereotyped motion of the robot that accelerates until the yoyo hits the bottom of the string and then returns to the initial position.

Open-loop analysis indicates that the steady working curve of the yoyo is a straight line passing through the origin in the $\Pi^* T^*$-plane. By investigating the working curves of the four oscillators, we have shown that only the iPLL oscillator may stabilize the periodic motion of the yoyo.

The return map of the closed-loop system with the iPLL has been derived. The fixed point

and the stability region in the parameter space have been determined analytically and verified by numerical simulations.

The work presented here may be extended to other periodic systems for which the working curve may be determined. In particular the results presented here holds directly when the resulting working curve is linear as in the case of the yoyo.

A. Open-loop versus closed-loop control

Some systems may generate stable periodic responses under periodic excitations even without any feedback (i.e. open-loop control). A damped mass-and-spring system, for example, may be excited with any periodic signal, while the bouncing ball [30], [31] and the hopping robot [32], [33], should be excited with specific periodic signals to generate stable periodic motion. Interestingly, Sternad and her colleagues [34], [35], [36] demonstrated that humans intuitively exploits the mechanism of open-loop stability when juggling a bouncing ball. Feedback control may still be introduced in such systems so that the steady state amplitude (or period) of the response tracks a reference value.

Like the yoyo, however, there are systems that do not generate stable periodic response with open-loop control. Designing a nominal trajectory that balance the energy loss in each cycle, as proposed in this paper and in [37], facilitates the closed-loop control of such systems, but is not sufficient by itself. The main purpose of feedback is to stabilize their periodic motion.

B. Model-based versus oscillator-based control

The model-based approach generally requires accurate state estimation and thus accurate output feedback. In contrast, the oscillator-based approach requires only the detection of specific events. In the case considered here, the natural feedback for model-based control is visual feedback, which entails computationally demanding image processing. In contrast, the oscillator-based approach involves simple detection of the peak force, which occurs when the yoyo hits the

bottom. Although the oscillator in the oscillator-based control may also be regarded as a "poor observer", the main distinction between the two approaches is that the former requires at least a sufficiently accurate structure of the model whereas the later does not. The oscillator-based approach provides a model-free low feedback rate control of open-loop unstable systems.

C. Significance of PLLs

This work extends previous developments of ONNs and investigates for the first time the role of PLLs in controlling rhythmic movements. We demonstrate that PLLs may enforce either input lagging or a unique input-leading phase relationship and that the later has specific control advantages. Thus, the unique temporal detection characteristics of PLLs [24], [18] are shown to provide control capabilities beyond those of directly coupled neural oscillators. These capabilities may facilitate the application of ONNs to event-driven control of dexterous manipulations [38].

Acknowledgment

This research is supported by the Technion V.P.R. Fund–Henry Gutwirth promotion of research fund and by the fund for the promotion of research at the Technion.

Appendix

I. Yoyo Analysis

We consider one motion cycle of the yoyo under the stereotyped action of the robot described by the switching algorithm (1). When the yoyo begins rolling down from the top, the robot initially waits and then it starts moving up in a constant acceleration as the yoyo keeps rolling down. As soon as the yoyo reaches the bottom, the robot returns to its origin smoothly and quickly before the yoyo reaches the next peak.

A. Yoyo cycle

The one-DOF model of the yoyo (4) can be solved explicitly to determine the motion of the yoyo during each interval *I*, *II* and *III* under the control algorithm (1). Considering the j-th cycle, the only necessary information is: (1) the initial peak amplitude Θ_j, and (2) the waiting ratio μ_j. The final state at the end of each interval serves as the initial state of the subsequent interval. The following two propositions state the amplitude of the next peak (i.e. the return map of the amplitude of the yoyo) and the duration of the last two intervals, respectively, without proof.

Proposition 3: Given the j-th amplitude Θ_j and the waiting time ratio μ_j, the consecutive amplitude Θ_{j+1} of the simplified yoyo (4) under control algorithm (1), satisfies

$$\Theta_{j+1} = f(\mu_j; \kappa, e_{eq})\Theta_j \tag{26}$$

where

$$f(\mu; \kappa, e_{eq}) = \kappa\varphi^2(\mu; \kappa) + \left(e_{eq}\sqrt{1 + (1-\mu)\kappa} + \kappa\varphi(\mu; \kappa)\right)^2 \tag{27a}$$

in which

$$\varphi(\mu; \kappa) = \frac{-\sqrt{\mu} + \sqrt{1 + (1-\mu)\kappa}}{1 + \kappa} \tag{27b}$$

Proposition 4: For the simplified yoyo (4) under control algorithm (1), given the j-th amplitude Θ_j and the waiting time ratio μ_j, the duration of each interval *II* and *III* is given, respectively, by

$$\begin{aligned} \mathit{II}_j &= f_2(\mu_j; \kappa)\Delta_j \\ f_2(\mu; \kappa) &= \varphi(\mu; \kappa) \end{aligned} \tag{28}$$

$$\begin{aligned} \mathit{III}_j &= f_3(\mu_j; \kappa, e_{eq})\Delta_j \\ f_3(\mu; \kappa, e_{eq}) &= e_{eq}\sqrt{1 + (1-\mu)\kappa} + \kappa\varphi(\mu; \kappa) \end{aligned} \tag{29}$$

where $\varphi(\mu, \kappa)$ is defined by (27b).

B. Equilibrium condition

Equation (26) may be regarded as a nonlinear open-loop discrete system with Θ as its state variable and μ as its control input. If μ takes the value μ^* such that

$$f(\mu^*; \kappa, e_{eq}) = 1 \tag{30}$$

then Θ retains its initial value. Indeed, we found that equation (30) has only two solutions both of which are real. One of them, $\mu^* = (1+\kappa)/\kappa > 1$ has no physical meaning. The other one is

$$\mu^* = \mu^*(\kappa, e_{eq}) = \frac{\big((1+e_{eq})\kappa - (1-e_{eq})\big)^2}{\big((1+e_{eq})^2\kappa + (1-e_{eq})^2\big)\kappa} \tag{31}$$

Figure 7 shows μ^* vs κ with e_{eq} as a parameter. Each curve is tangent to the κ axis at

$$\kappa_0 = \frac{1-e_{eq}}{1+e_{eq}} \tag{32}$$

When $\kappa < \kappa_0$, $f(\mu;\kappa) < 1$ for all $\mu \in [0,1]$. This implies that the energy cannot be balanced and hence the dotted part (for $\kappa < \kappa_0$) of each curve in Fig. 7 has no physical significance.

(Fig. 7 here)

C. Working curve

In steady state, the ratio of $\mathit{\Pi}^*$ and T^* is given by

$$\upsilon(\kappa, e_{eq}) \triangleq \frac{\mathit{\Pi}^*}{T^*} = \frac{f_2(\mu^*;\kappa)}{f_1(\mu^*) + f_2(\mu^*;\kappa) + f_3(\mu^*;\kappa)} \tag{33}$$

By substituting μ^* given by (31) into f_1, f_2 and f_3 given by (11), (28) and (29) respectively, the explicit ratio given by (8) is derived.

References

[1] A. H. Cohen, S. Rossignol, and S. Grillner, Eds., *Neural Control of Rhythmic Movements in Vertebrates*, John Wiley, Canada, 1988.

[2] S. Grillner, "Locomotion in vertebrates: Central mechanisms and reflex interaction," *Physiological Reviews*, vol. 55, no. 2, pp. 247–304, Apr. 1975.

[3] S. Grillner, "Neurological bases of rhythmic motor acts in vertebrates," *Science*, vol. 228, pp. 143–149, 1985.

[4] M. L. Shik and G. N. Orlovsky, "Neurophysiology of locomotor automatism," *Physiological Reviews*, vol. 56, no. 3, pp. 465–501, July 1976.

[5] P. S. G. Stein, "Motor systems, with specific reference to control of locomotion," *Annual review of Neuroscience*, vol. 1, pp. 61–68, 1978.

[6] J. J. Collins and S. A. Richmond, "Hard-wired central pattern generators for quadrupedal locomotion," *Biological Cybernetics*, vol. 71, pp. 375–385, June 1994.

[7] P. F. Rowat and A. I. Selverston, "Modeling the gastric mill central pattern generator of the lobster with a relaxation-oscillator networks," *Journal of Neurophysiology*, vol. 70, no. 3, pp. 1030–1053, Sept. 1993.

[8] S. Grillner, P. Wallen, L. Bordin, and A. Lansner, "The neural network generating behavior in lamprey—circuitry, transmitters, membrane properties, and simulation," *Annual Review of Neuroscience*, vol. 89, pp. 31–35, 1988.

[9] H. Haken, J. A. S. Kelso, and H. Bunz, "A theoretical model of phase transitions in human hand movements," *Biological Cybernetics*, vol. 51, pp. 347–356, 1985.

[10] J. Yamanishi, M. Kawato, and R. Suzuki, "Two-coupled oscillators as a model for the coordinated finger tapping by both hands," *Biological Cybernetics*, vol. 37, pp. 219–225, 1980.

[11] Z. Teresa, "Coupled oscillators utilized as gait rhythm generators of a two-legged walking machine," *Biological Cybernetics*, vol. 74, pp. 263–273, 1996.

[12] H. J. Chiel, R. D. Beer, R. D. Quinn, and K. S. Espenschied, "Robustness of a distributed neural network controller for locomotion in a hexapod robot," *IEEE Transactions on Robotics and Automation*, vol. 8, no. 3, pp. 293–303, June 1992.

[13] M. F. Cao and K. Atsuo, "A design method of neural oscillatory networks for generation of humanoid biped walking patterns," in *Proceedings of the IEEE International Conference on Robotics and Automation*, Leuven, Belgium, May 1998, vol. 3, pp. 2357–2362.

[14] A. Lansner and O. Ekeberg, "Neural network models of motor generation and control," *Current Opinion in*

Neurobiology, vol. 4, pp. 903–908, 1994.

[15] U. Bassler, "On the definition of central pattern generator and its sensory control," *Biological Cybernetics*, vol. 54, pp. 65–69, 1986.

[16] F. Delcomyn, "Neural basis of rhythmic behavior in animals," *Science*, vol. 210, pp. 492–498, 1980.

[17] E. Ahissar, S. Haidarliu, and M. Zacksenhouse, "Decoding temporally encoded sensory input by cortical oscillations and thalamic phase comparators," *Neurobiology*, vol. 94, pp. 11633–11638, Oct. 1997.

[18] M. Zacksenhouse, "Sensitivity of basic oscillatory mechanism for pattern generation and detection," *Biological Cybernetics*, vol. 85, pp. 301–311, 2001.

[19] H. Kimura, S. Akiyama, and K. Sakurama, "Realization of dynamic walking and running of quadruped using neural oscillators," *Autonomous Robots*, vol. 7, no. 3, pp. 247–258, Nov. 1999.

[20] N. G. Hatsopoulos, W. H. Warren, and J. N. Sanes, "A neural pattern generator that tunes into the physical dynamics of the limb system," in *Proceedings of the International Joint Conference on Neural Nerowrks*, Baltimore, MD, May 1992, vol. 1, pp. 104–109.

[21] N. G. Hatsopoulos, "Coupling the neural and physical dynamics in rhythmic movements," *Neural Computation*, vol. 8, pp. 567–581, 1996.

[22] M. M. Williamson, "Neural control of rhythmic arm movements," *Neural Networks*, vol. 11, pp. 1389–1394, 1998, 1998 Special Issue.

[23] C. Koch and I. Segev, Eds., *Methods in Neuronal Modeling*, MIT press, Cambridge, MA, 1989.

[24] F. M. Gardner, *Phaselock Techniques*, John Wiley, Canada, 1979.

[25] E. Ahissar, "Temporal-code to rate-code conversion by neuronal phase-locked loops," *Neural Computation*, vol. 10, pp. 597–650, 1998.

[26] E. M. Izhikevich, "Weakly pulse-coupled oscillators, fm interactions, synchronization, and oscillatory associative memory," *IEEE Transactions on Neural Networks*, vol. 10, no. 3, pp. 508–526, 1999.

[27] H. L. Jin and M. Zacksenhouse, "Yoyo dynamics: Sequence of collisions captured by a restitution effect," *Journal of Dynamic Systems, Measurement and Control*, Sept. 2002, (in press).

[28] H. L. Jin and M. Zacksenhouse, "Necessary condition for simple oscillatory neural control of robotic yoyo," in *International Joint Conference on Neural Nerowrks-World Congress on Computational Intelligence (IJCNN-WCCI'02)*, Honolulu, HI, May 2002, pp. 1427–1432.

[29] K. J. Astrom and B. Wittenmark, *Computer Controlled System*, Prentice-Hall Inc., Englewood Cliffs, H.J., 1984.

[30] J. Guckenheimer and P. Holmes, *Nonlinear Oscillations, Dynamical system, and Bifurcations of Vector Fields*, Springer-Verlag, NY, 1983.

[31] S. Schaal and C. G. Atkeson, "Open-loop stable control strategies for robot juggling," in *Proceedings of the IEEE International Conference on Robotics and Automation*, Atlanta, GA, May 1993, vol. 3, pp. 913–918.

[32] D. E. Koditschek and M. Buehler, "Analysis of a simplified hopping robot," *The International Journal of Robotics Research*, vol. 10, no. 6, pp. 587–605, Dec. 1991.

[33] H. Komsuoglu and D. E. Koditschek, "Preliminary analysis of a biologically inspired 1-dof 'clock' stabilized hopper," in *Proceedings of World Multiconference on Systemics, Cybernetics and Informatics (SCI2000)*, Orlando, FL, July 2000, vol. 4, pp. 670–675.

[34] S. Schaal, C. G. Atkeson, and D. Sternad, "One-handed juggling: A dynnamic approach to a rhythmic movement task," *Journal of Motor Behavior*, vol. 28, no. 2, pp. 165–183, 1996.

[35] D. Sternad, M. Duarte, and S. Schaal, "Dynamics of a bouncing ball in human performance," *Physical Review E*, vol. 63, pp. 011902.1–8, 2000.

[36] D. Sternad and H. Katsumata, "Dynamic stability in the acquisition and aerformance of a rhythmic skill: An example for a perception-action approach," *Journal of Human Kinetics*, vol. 4, pp. 57–73, 2000.

[37] K. Hashimoto and T. Noritsugu, "Modeling and control of robot yoyo with visual feedback," in *Proceedings of the IEEE International Conference on Robotics and Automation*, Minneapolis, MN, Apr. 1996, vol. 3, pp. 2650–2655.

[38] J. M. Hyde and M. R. Cutkosy, "A phase management framework for event-driven dextrous manipulation," *IEEE Transactions on Robotics and Automation*, vol. 14, no. 6, 1998.

List of Figures

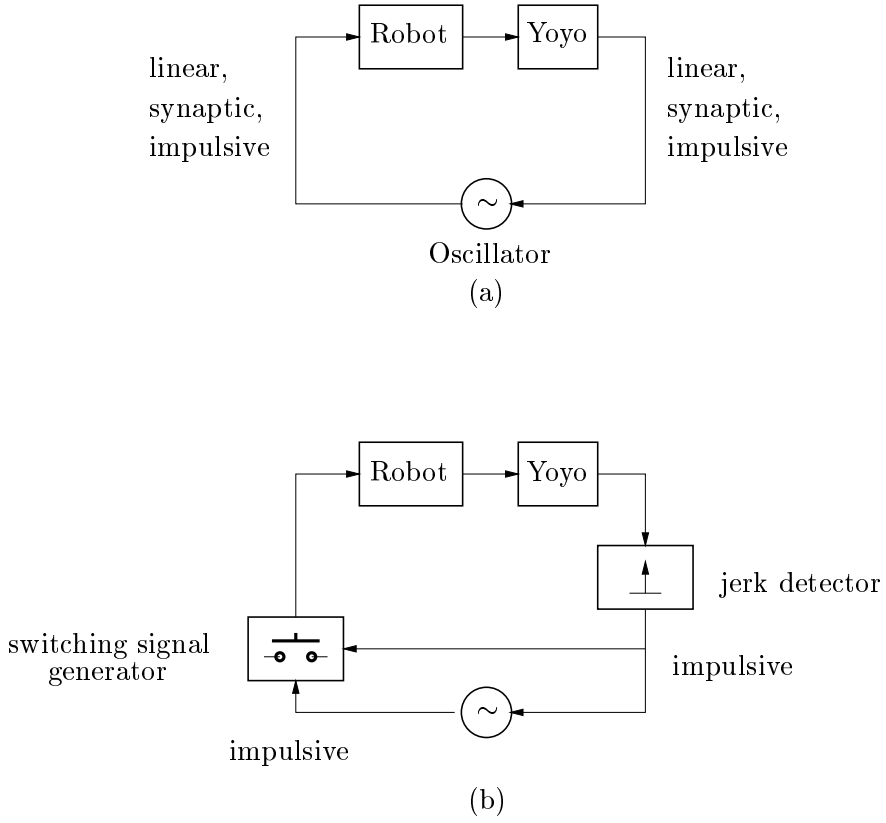

Fig. 1. Oscillatory yoyo control in general (a) and the specific configuration studied here (b)

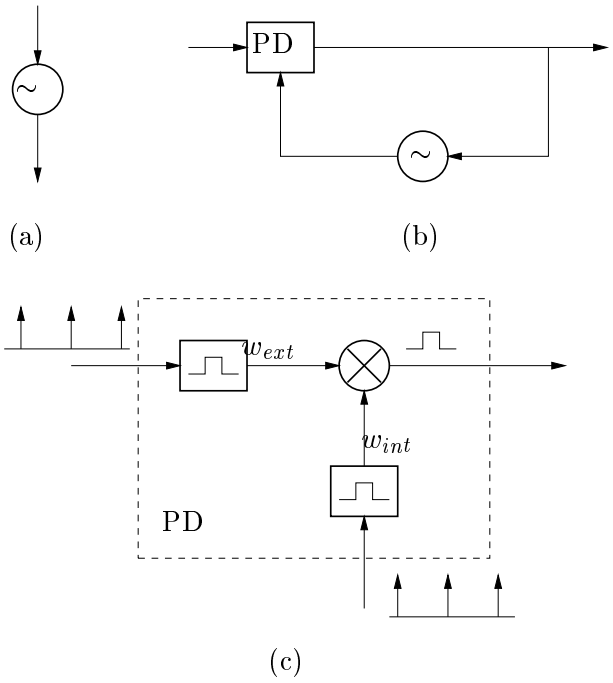

Fig. 2. Simple oscillator (a), Phase locked loop (b), and Phase detector (c)

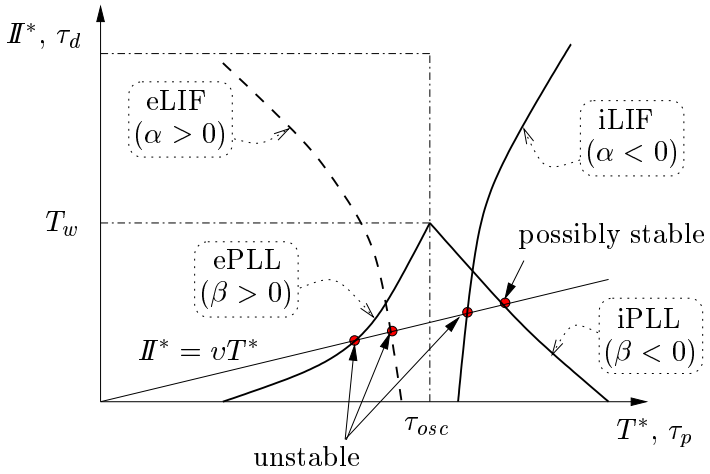

Fig. 3. The working curve of the yoyo and its intersections (marked by circles) with those of the oscillators

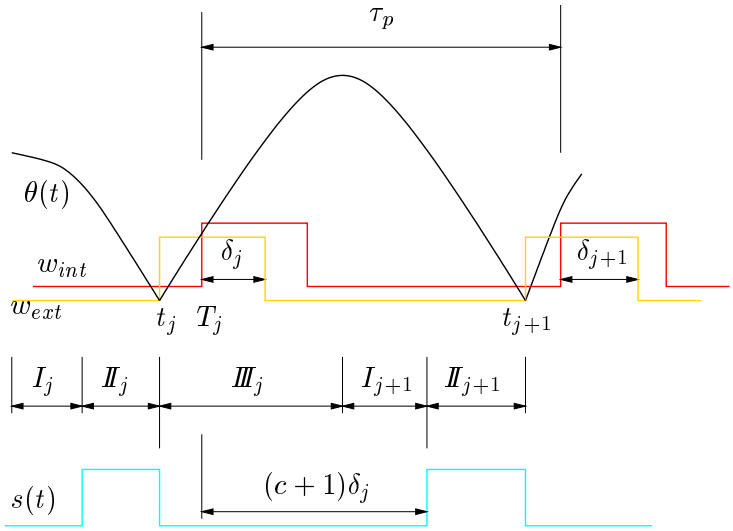

Fig. 4. The waves of a controlled yoyo ($c = 2$)

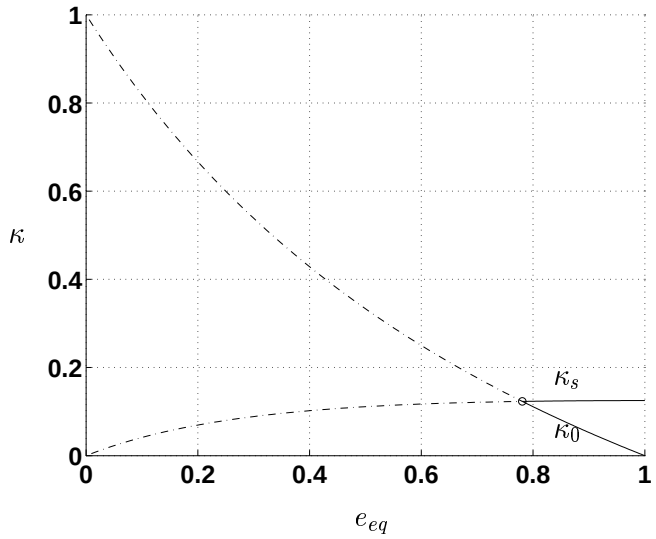

Fig. 5. Stability region: $\kappa_0 < \kappa < \kappa_s$

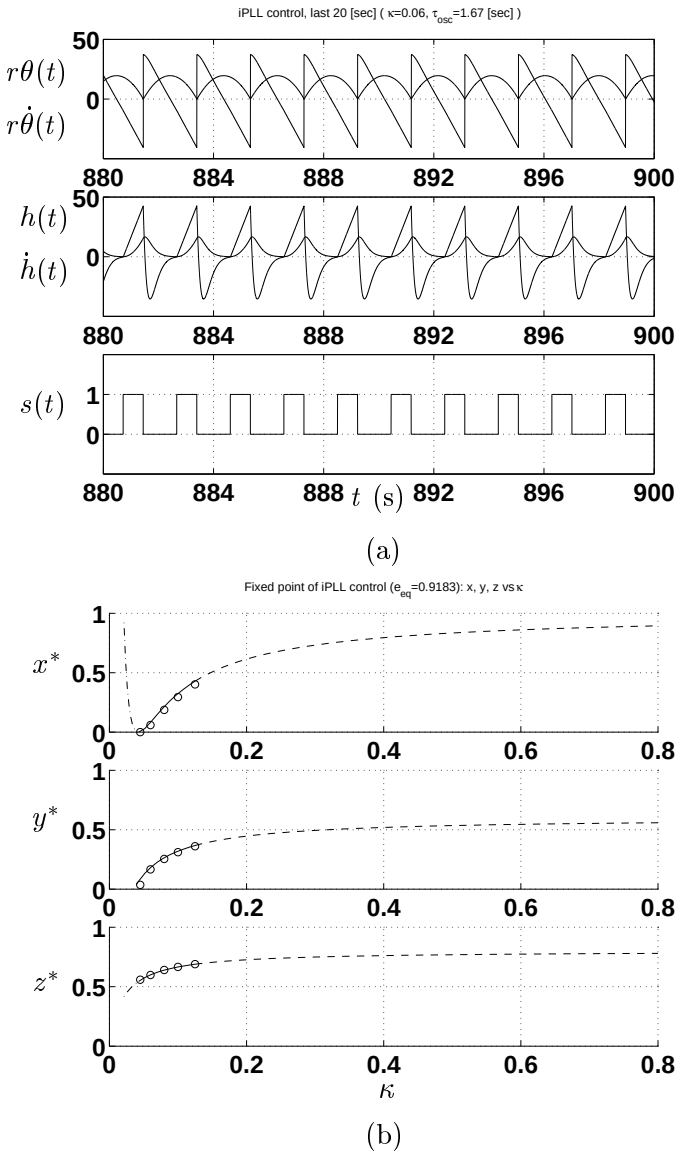

Fig. 6. Control simulation (Yoyo-1, $e_{eq} = 0.9183$, $\gamma = 0.0817$): (a) Last 20 s of the response (for $\kappa = 0.06$, $\tau_{osc} = 1.67$ s), and (b) Comparison of numerical (circles) and theoretical values (line) of the fixed point (x^*, y^*, z^*) versus κ.

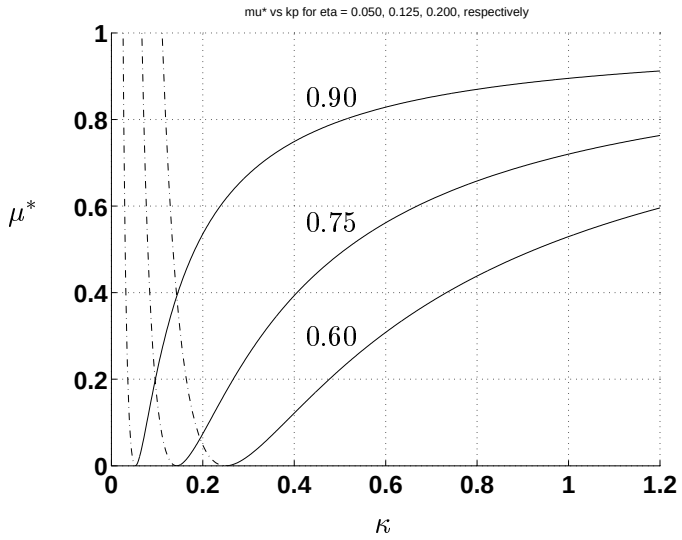

Fig. 7. μ^* vs κ for three different e_{eq}